2016 IEEE-RAS 16th International Conference on
Humanoid Robots (Humanoids)
Cancun, Mexico, Nov 15-17, 2016

Convexity of Stiffness Matrix Eigenvalues for a Position Controlled Limb of Mobile Climbing Robots

Xuan Lin and Dennis W. Hong

Abstract— **This paper presents a simple model of the structure stiffness of a position controlled limb designed for mobile climbing robot. The stiffness matrices of the robot limb at different configurations are investigated. Experiments are conducted to demonstrate that this model is able to predict the general trend of change of stiffness matrix as a function of end effector position. Experiments also show that the maximum eigenvalue of stiffness matrix is a convex function with respect to the effector position, which matches the prediction of theory. Other testing includes measuring the effect of motor backlash on stiffness coefficients, and gauge the amount of contribution to total compliance from joint compliance and structure compliance.**

I. Introduction

Position control is a simple and widely used control law for robot limbs which only controls the joint angle to reach the desired position. Force control is also a commonly used control law. The idea behind force control is, with fixed configuration, to actively control the stiffness in order to generate the desired reaction force [1][2][3]. Force control needs force sensor installed to give feedback, which can make the system complicated, so sometimes position control is preferred. For position control, the stiffness is fixed at a given configuration. However, we can still select the desired stiffness by selecting limb configurations. Since the compliance of structures differ at different direction (especially for composites), the stiffness can change considerably at different configurations. This motivates the idea of stiffness optimization and planning.

Consider a multi-limbed robot doing free climbing [4], which only depends on friction at contact points to support its body. An example is shown in Figure 1. Since a climbing robot usually have 3 or more contact points, the contact force is indeterminate [5], which means the stiffness of robot limbs must be considered to solve the contact force exactly. Previous works can be seen in [6][7]. If the payload of the robot is given, we can have a reasonable gauge of the robot center of mass sag down, i.e. the deflection of each limb can be estimated. Thus, one way to solve the motion planning problem for climbing robots is to treat it as a stiffness planning problem. Each robot limb picks a contact point with proper stiffness to satisfy the friction cone constraint. An idea is demonstrated in Figure 2. The robot body has a sag down due to the load, which creates a contact force on the toe. On the left hand side, the limb has small K_{xz}, thus less friction is needed to hold the toe in position. While on the right hand side, the limb has larger K_{xz}, thus is easier to slide.

In this paper, we explore the stiffness properties for an anisotropic composite (carbon-fiber) based robot limb. A simple model of the structure stiffness for a robot limb is presented. Unlike the works [8], this model is graph based, thus is intuitive and requires minimum linear algebra background to understand. The model shows the general trend of the stiffness matrix with respect to the change of end effector position. The parameters in the model - compliance ellipsoid – can easily be experimentally identified. Specifically, we show that a common measure of the stiffness matrix, eigenvalues, demonstrates convexity w.r.t. end effector position, which is potentially useful for stiffness optimization and planning. Experiments are designed to verify the theory, as well as testing the motor backlash. We only explore the 2D stiffness matrix for a planar limb here, future work will generalize this method to a 3D limb.

It is also notable here that different from similar works on common industrial robots [9], and common flexible manipulators [10][11], our limb is designed for mobile climbing robot. Some parts of the structure are intentionally made thin in order to save weight, but the whole structure is still rigid enough to support the robot body. In fact, the maximum deflection imposed in our experiment is 2.5mm, which is about 1% of the arm length, so linear elasticity law should be satisfied. The climbing process is assumed to be quasi-static, so structure dynamics is not considered in this paper.

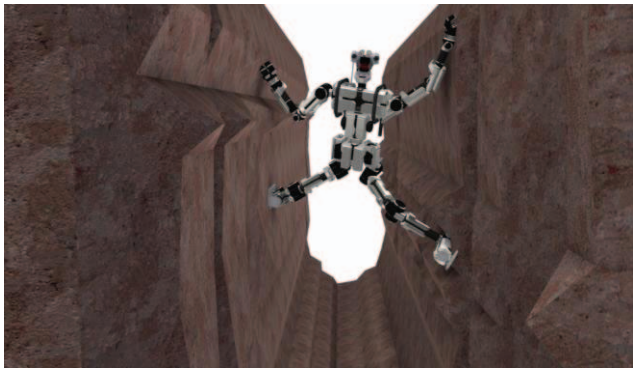

Figure 1 Robot Bracing at Cliff

Xuan Lin is a graduate student in University of California, Los Angeles
Dennis W. Hong is a professor in Department of Mechanical and Aerospace Engineering, University of California, Los Angeles

Authorized licensed use limited to: UCLA Library. Downloaded on May 10,2020 at 19:46:24 UTC from IEEE Xplore. Restrictions apply.

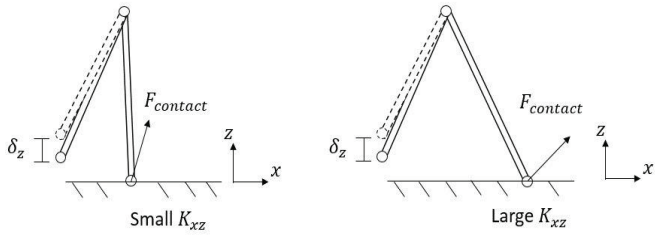

Figure 2 Choice of Stiffness Coefficients

II. Previous Work

Many researches have been done to model the stiffness property of manipulators. [12] Establishes the stiffness map in the workspace of a manipulator, and helps the designer to avoid the zone where the stiffness is not acceptable. [13] presents a mathematical way to identify the stiffness of joints, and further the complete stiffness of the robot manipulator. Many previous papers on industrial manipulators claims that the major part of flexibility comes from joint gear boxes, thus only models and identify gear compliance [14]. But for our robot structure rigidity does come into play, especially when the structure is fully folded or stretched out. Also, for mobile robots, even if the structure is rigid, we want to know how rigid it is, which is useful to calculate the amount of body sag down and the resultant contact force. [6][7] Models the pantograph type manipulator into beams, and calculate the stiffness matrix by Castigliano's theorem. The algebra explicitly shows the connection of stiffness matrix to the joint angles. As we can see, the analytical expression for stiffness matrix is complicated, and the intuition behind it is obscured. In order to do stiffness optimization, a simple and easily achievable function is preferred. Furthermore, if the problem has good mathematical properties (e.g. convexity), fast and stable algorithms exist to solve the optimization problem.

Stiffness matrices are positive definite. Eigenvalues of a positive definite matrix are all positive, and are unitary invariant, which means invariant under matrix rotations. Also, the maximum and minimum eigenvalues of a stiffness matrix give upper and lower bounds of how much the matrix can amplify the magnitude of a deflection vector, thus provide information on the resultant contact force. In the following sections, we further explore the general trend of stiffness matrix eigenvalues, and demonstrate that they have a good property of convexity w.r.t end effector position.

III. Stiffness Matrix with respect to Joint Angles

Figure 3 is a picture of the robot limb being investigated. It is a 3 degree of freedom limb, with 3 sections called coxa, femur, tibia, and 3 joints called joint 1, 2, 3, respectively. The rod connecting motors are made of carbon fiber tubes. Other holding parts are made up of aluminum. The length of coxa section is 57mm, femur section is 185mm, and tibia section is 313.5mm. The motors are dynamixel 106s, with a gear reduction ratio 225:1. This means the joint compliance is an important part of the total compliance. The idea behind the model presented in this paper is motivated by structure compliance. This model is generalizable to total compliance (structure compliance plus joint compliance) but with some flaws mentioned in the page 4.

Since the robot limb has a point contact, no torque is imposed at end effector. Therefore, the stiffness matrix can be reduced to a 3 by 3 stiffness matrix. Furthermore, we only consider planar manipulation here, hence joint 1 is considered to be fixed, and the stiffness matrix being interested in is a 2 by 2 matrix.

Following previous works, we model the robot limb structure into a series of beams, as shown in Figure 4.

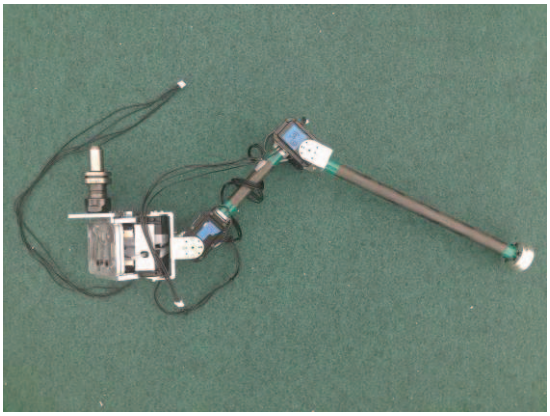

Figure 3 Robot Limb

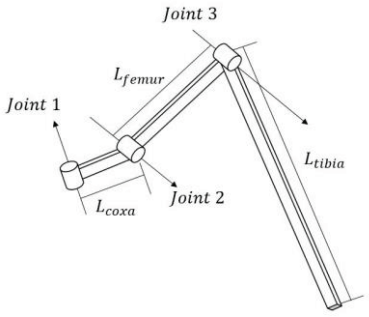

Figure 4 Model of Robot Limb

Since we are doing position control - controlling end effector position by joint angles, we are interested in how the change of end effector position affects the eigenvalues of stiffness matrix at end effector. i.e. we are interested in

$$\lambda_K(\underline{p}_{EF/O})$$

Where $\underline{p}_{EF/O}$ is the position vector of end effector, and λ_K are eigenvalues of the stiffness matrix.

Since $\underline{p}_{EF/O}$ is connected to the joint angles $\underline{\theta}$ by inverse kinematics (IK, can be written as $\underline{\theta}(\underline{p}_{EF/O})$), we can start by

Authorized licensed use limited to: UCLA Library. Downloaded on May 10,2020 at 19:46:24 UTC from IEEE Xplore. Restrictions apply.

exploring the functional property of $\lambda_K(\underline{\theta})$, and then put the inverse kinematics back later to complete $\lambda_K(\underline{p_{EF/O}})$.

According to the well-known Maxwell-Betti reciprocal theorem [15], in a linearly elastic system subject to discrete loads at point A, the stiffness matrix and compliance matrix (inverse of stiffness matrix) at point A is always a symmetric matrix. In practice, it is valid to assume that this matrix is always positive definite (if not so, then there will be at least 1 negative eigenvalue, which means at some direction the material deforms opposite to load – counterintuitive). According to linear algebra, a 2 by 2 positive definite matrix will have 2 strictly positive eigenvalues. The largest and smallest eigenvalues give upper and lower bound of the amplification of contact force magnitude. To explain in greater details, the definition of stiffness matrix is

$$\boldsymbol{f = K\delta} \tag{1}$$

Where δ is the deflection vector, K is the stiffness matrix, and f is the resultant contact force vector. For any positive definite matrix, we have

$$\boldsymbol{\lambda_{min}(K)\|\delta\| \leq \|K\delta\| \leq \lambda_{max}(K)\|\delta\|} \tag{2}$$

Where $\lambda_{min}(K)/\lambda_{max}(K)$ are the smallest/largest eigenvalues of K, respectively. Therefore, with the knowledge of eigenvalues, we retrieve information of the magnitude of contact force.

Maxwell-Betti theorem also tells us one important thing: if we pick a piece of material and impose load at only one point, the stiffness of the material as seen by that load can be deemed as an ellipsoid (named compliance ellipsoid in this paper). This is a direct result from that each positive definite matrix has an ellipsoid associated with it, and motivates the idea of using ellipsoids to model the compliance of robotic limb. Figure 5 is a 2-dimensional beam element and its 2 by 2 compliance matrix and the corresponding ellipsoid plotted. If the load imposed at point A is along direction 1, it sees a small compliance coefficient, corresponding to the smallest eigenvalue; if the load is imposed along direction 2, it sees a large compliance coefficient, corresponding to the largest eigenvalue. If the load starts to rotate, the compliance coefficient it sees comprises of the surface of ellipsoid.

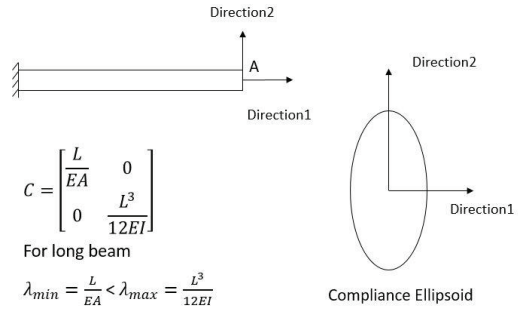

Figure 5 2-D Beam Element and Compliance Ellipsoid

Now, let's put two beam elements together, and load it along a fixed direction. What if we change the joint angle, θ_2, i.e. beam element 1 is fixed but beam element 2 is rotating? Due to linear elasticity assumption, the total compliance matrix is a summation of that of each element. i.e.

$$\boldsymbol{\delta = \delta_1 + \delta_2 = C_1 f + C_2 f} \tag{3}$$

Note equation (3) is only true when the torque is not taking into account. Figure *6* shows a diagram of two beam limb with one rotating and the other one fixed, and Figure *7* shows the force and compliance analysis for each beam element.

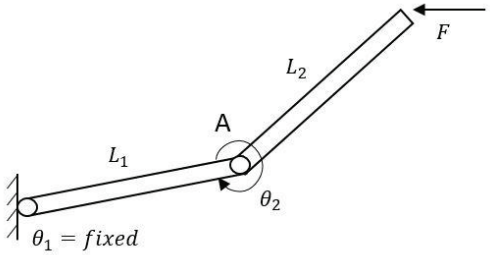

Figure 6 Two Beam Limb

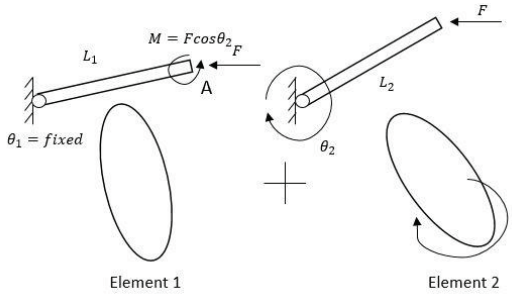

Figure 7 Analysis of Each Element

We see that since element 2 is rotating, compliance ellipsoid 2 is rotating. Therefore, the total compliance ellipsoid is the summation of a fixed compliance ellipsoid and a rotating compliance ellipsoid. If the direction of largest eigenvalue aligns up, the total compliance ellipsoid will be "stretched" (the large eigenvalue is large, the small eigenvalue is small), while if the direction of largest eigenvalue for ellipsoid 1 aligns with the smallest eigenvalue for ellipsoid 2, the total compliance ellipsoid will be more "circle like" (the large eigenvalue is small, the small eigenvalue is large). With this intuition in mind, it is easy to see that the largest/smallest eigenvalue as a function of θ, i.e. $\lambda_K(\underline{\theta})$, will demonstrate a peak/valley shape.

We want to highlight here that a structure component can always be modeled into ellipsoids no matter what geometry it takes. This is useful for model identification since the structure can be made by nontrivial materials (e.g. composites) and take complicated geometries, thus the theoretical derivation in [6][7] won't work well. When resort to experiments, a unified model allows one to reconstruct an analytical expression for stiffness/compliance matrix using minimal times of experiments.

As one may notice, this model fails to describe the deflection caused by the pure moment $F\cos\theta_2$ imposed at

Authorized licensed use limited to: UCLA Library. Downloaded on May 10,2020 at 19:46:24 UTC from IEEE Xplore. Restrictions apply.

point A. What this model says is the compliance of element 1 is only a function of θ_1, while the compliance of element 2 is only a function of θ_2. However, due to the moment transfer between elements, the compliances are coupled, i.e. a change of θ_2 will change the effective compliance of element 1, and cause a deformation of the compliance ellipsoid. Similarly, when we put joint compliance into consideration and model it as torsional springs, this model is able to incorporate the torsion caused by F at point A, but not the part caused by $F\cos\theta_2$. Therefore, when experimentally identify the model parameters, we need to compensate for that.

Now a functional relation of $\lambda_K(\underline{\theta})$ is achieved, we put IK $\underline{\theta}(\underline{p}_{EF/O})$ back to get $\lambda_K(\underline{p}_{EF/O})$.

For the limb we are working on, the first section (coxa) is comparatively short, thus its deformation is ignored, and assume the first two rotational axes are intersecting with each other. The result configuration naturally fits into a spherical coordinate system. Since this paper only considers planar manipulation, a polar coordinate system is set up, as shown in Figure *8*. The kinematic parameter, r, describes how much the robot limb "reach out", while the kinematic parameters φ describe how the limb rotates spatially. The definition of joint angles is also shown.

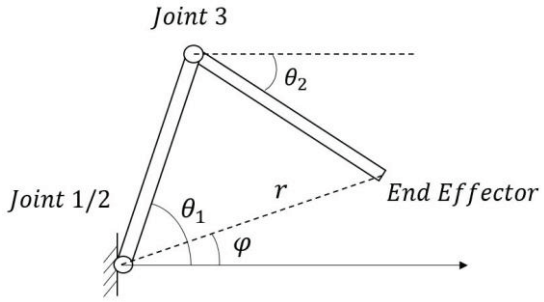

Figure 8 Robot Limb in Polar Coordinate System

In section 3 we find out that for two beams, the compliance ellipsoid can be "stretched" or "circle like" depending on their configuration. For long beams, their axial stiffness is much larger than their vertical stiffness, and this is particularly true for carbon fibers, since the fiber direction is along the axial direction, making it extremely strong axially. Therefore, when the axial direction of two beams aligns up, the limb is very stiff along axial direction, while very compliant along vertical direction. When they are at a 90 degree angle, the limb is equally stiff/compliant along two directions.

Now, when the robot limb stretches out, its configuration continues to change from align up (folded) to at a 90-degree angle to align up (fully stretched) again. So the largest/smallest eigenvalue will demonstrate again a peak/valley curve with respect to the coordinate parameter, r. Figure 9 shows 3 intermediate configurations as the limb reaches out, along with their compliance ellipsoids. The eigenvalues are also depicted. By virtue of Castigliano's theorem [16], we construct a simple model for the limb we are using, and the eigenvalues are computed. Figure 10 plots the resultant curve of maximum/minimum eigenvalues of stiffness matrices. Note here that we plot the eigenvalues of stiffness matrices to be comparable to the experiment results. If we recall the definition of quasi-convexity [17], the $\lambda_{min}(K)$ / $\lambda_{max}(K)$ function is quasi-convex/concave with respect to r (for λ_{max}, it is actually convex). This feature can be used for doing stiffness optimization.

Note here that when the limb reaches out, the joint angle θ_2 only ranges from 0 to 180 degrees, thus only 1 peak/valley is observed and result in quasi-convexity.

Additionally, rotate angle φ doesn't change the eigenvalue of stiffness matrix, since eigenvalues are invariant under matrix rotation.

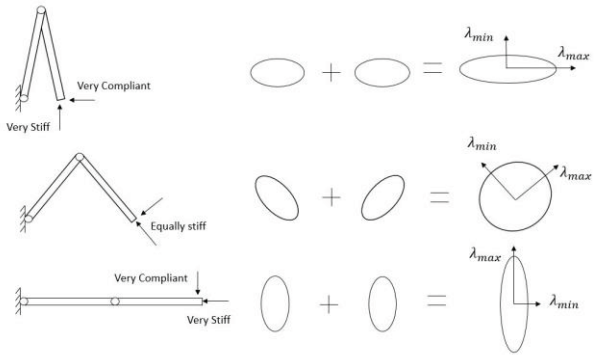

Figure 9 Stiffness of 2 Element Limb at Different Configurations

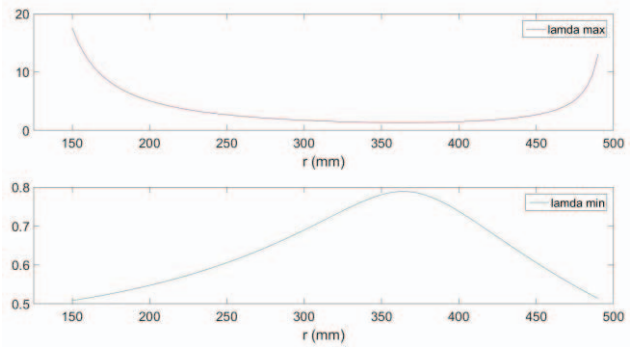

Figure 10 Largest/Smallest Eigenvalue of Stiffness Matrix w.r.t Kinematic Parameter r

IV. Experiment Results

In order to test the theoretical results, experiments are established to measure the stiffness matrix of the robot limb. The experiment is done on a 3 axis CNC machine. Figure *11* illustrates our setup. The robot limb is fixed at point A through the machine gripper, while hinged at point B by a ball joint. This ball joint ensures that no moment can be transferred from the fixture, thus simulate a pure friction contact. The ball joint is connected to the vise, which can move relative to the gripper at 3 axes. The z axis is along vertical direction, with positive upwards, while the x axis is along horizontal direction, with positive to the right. The amount of displacement is controlled by the machine. If we displace the robot limb along one axis, we get reaction force at end effector,

Authorized licensed use limited to: UCLA Library. Downloaded on May 10,2020 at 19:46:24 UTC from IEEE Xplore. Restrictions apply.

which is measured by a ATI mini45 6 axes force/torque sensor. By doing single axis loading test, we can retrieve 2 components in the stiffness matrix. Therefore, through 2 axes loading test, we are able to build the 2 by 2 stiffness matrix. When the single axis test is conducted, point A and B are shift relative to each other up to 2 inch, with a 0.025-inch step, thus 8 data points are measured.

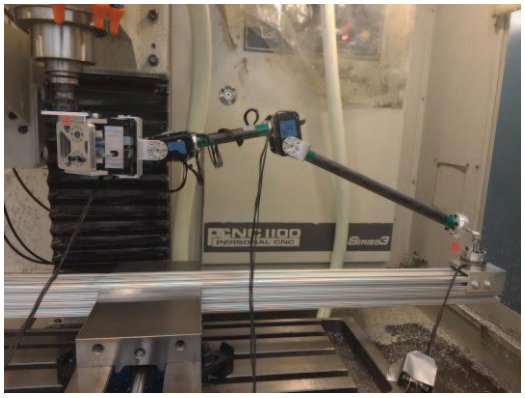

Figure 11 Experiment Setup

First, a cycle loading test is conducted to test the impact of backlash. Starting from zero load condition, the limb is loaded 2 inch along $-Z$ direction first, and gradually unload and load 2 inch along $+Z$ direction. The reaction force is measured at 0.025-inch step. One set of data is depicted in Figure 12, measured at $\theta_1 = 70°$ and $\theta_2 = 50°$. It is noticed that when unloaded, the 0 reaction force point is shifted. The experiment is repeated several times, and this phenomenon reappears with the same amount of loading, thus the author thinks it's due to the motor backlash (instead of plastic deformation). We can tell from Figure 12 that for the robot of our size, the zero reaction force point can shift 2.5mm due to backlash. This issue needs to be taken into consideration when the robot is climbing like Figure 1.

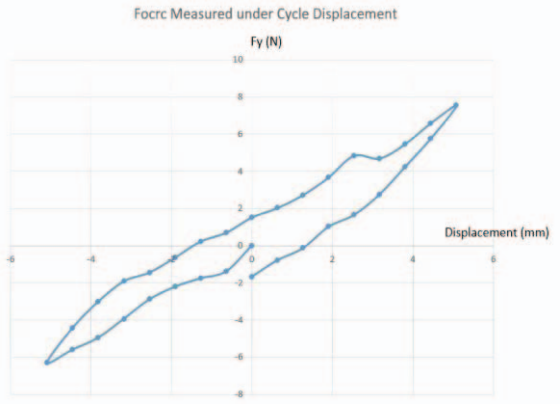

Figure 12 Cycle Load Test

Since the motor has a backlash, the joints are preloaded to get rid of it when we measure stiffness matrices. The preload is subtracted out from the data points, and the slopes are averaged to compute stiffness coefficients, i.e.

$$k = \frac{1}{\mathrm{n}}\sum_{i=1}^{\mathrm{n}} \frac{F - F_{preload}}{\delta - \delta_{preload}}$$

We load the robot limb at 12 different configurations, the result is listed in table I. The result eigenvalue curves are plotted in Figure 13. All testes are repeated at least twice to make sure the data are repeatable. Stiffness matrix K is put as $\begin{bmatrix} K_{xx} & K_{xz} \\ K_{zx} & K_{zz} \end{bmatrix}$.

TABLE I. EXPERIMENT DATA

	r (mm)	K(N/m)	λ_{min}	λ_{max}
1	158	$\begin{bmatrix} 0.5 & -1.7 \\ -1.7 & 11.0 \end{bmatrix}$	0.2316	11.2684
2	176	$\begin{bmatrix} 1.0 & -2.0 \\ -2.0 & 8.5 \end{bmatrix}$	0.5	9
3	222	$\begin{bmatrix} 1.0 & -2.0 \\ -2.0 & 5.0 \end{bmatrix}$	0.1716	5.8284
4	236	$\begin{bmatrix} 1.3 & -1.8 \\ -1.8 & 3.0 \end{bmatrix}$	0.1594	4.1406
5	242	$\begin{bmatrix} 1.2 & -1.5 \\ -1.5 & 2.2 \end{bmatrix}$	0.1189	3.2811
6	276	$\begin{bmatrix} 2.5 & -2.7 \\ -2.7 & 3 \end{bmatrix}$	0.0385	5.4615
7	303	$\begin{bmatrix} 2.0 & -2.0 \\ -2.0 & 2.1 \end{bmatrix}$	0.0494	4.0506
8	320	$\begin{bmatrix} 1.7 & -2.0 \\ -2.0 & 3.0 \end{bmatrix}$	0.247	4.453
9	437	$\begin{bmatrix} 5.0 & -1.1 \\ -1.1 & 0.9 \end{bmatrix}$	0.6235	5.2765
10	458	$\begin{bmatrix} 5.5 & -1.4 \\ -1.4 & 0.5 \end{bmatrix}$	0.1347	5.8653
11	481	$\begin{bmatrix} 15.0 & -2.3 \\ -2.3 & 0.4 \end{bmatrix}$	0.0462	15.3538
12	484	$\begin{bmatrix} 18.0 & -5.0 \\ -5.0 & 1.6 \end{bmatrix}$	0.1958	19.4042

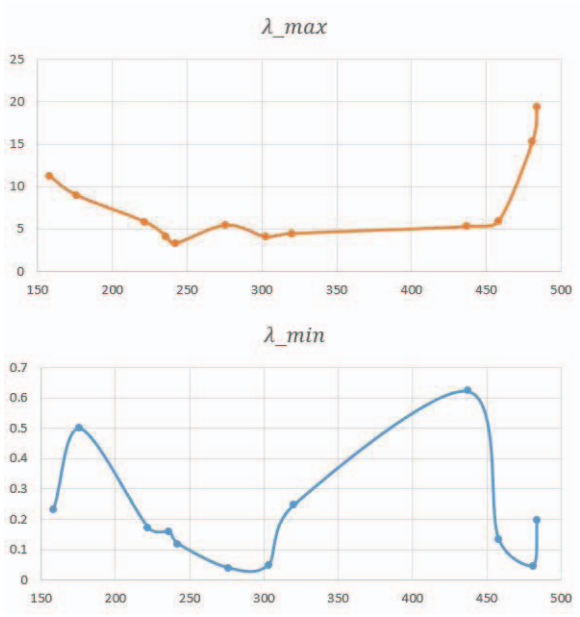

Figure 13 Experimentally Determined Eigenvalue curve

Authorized licensed use limited to: UCLA Library. Downloaded on May 10,2020 at 19:46:24 UTC from IEEE Xplore. Restrictions apply.

We can tell from the experiment result that the stiffness coefficients do depend considerably on limb configurations. For example, K_{xx} in configuration 11 is 30 times as much as it is in configuration 1. For eigenvalues, the maximum eigenvalue does approximately show a convex curve as the limb is stretching. However, the minimum eigenvalue doesn't follow the theoretical result in Figure 10, it actually vibrates as r increases. In fact, some numbers in the middle part (configuration 3 to 8) doesn't appear to be monotonic, especially those K_{xz} values. There may be several reasons. The model doesn't consider deflection caused by pure moment $F\cos\theta_2$ at point A in Figure 7, and we do notice a considerable sensor measurement noise.

Although the idea behind this model is motivated by structure compliance, it will be valuable to gauge what portion of compliance ellipsoid is actually contributed by structure compliance instead of joint compliance. By assuming that the all structure elements are perfectly rigid, and model the joint compliance into torsional springs with stiffness coefficients K_1 and K_2, one can derive analytical expression for compliance matrix induced only by joint compliance. From 2 sets of experiment data, K_1 and K_2 can be identified, and pure joint compliance matrices are computed to compare to experiment data. With this method, we roughly gauge the structure compliance to comprise to 30% of the total compliance.

V. Conclusion and Future Work

This paper investigates the stiffness properties of a position controlled limb at different configurations, specifically, a typical measure of the stiffness matrix – eigenvalues. The theory predicts that the stiffness coefficients vary considerably at different limb configurations. Furthermore, the maximum/minimum eigenvalues demonstrate quasi-convexity/concavity with respect to kinematic parameter, r. The experiment result shows that for our robot limb, stiffness coefficient can vary 30 times at different configurations. Also, the maximum eigenvalue is approximately a convex function of kinematic parameter r, but the minimum eigenvalue is not as good characterized. These experiments help us to understand the role which the stiffness of robot limb plays when a multi-limbed robot is doing on-wall motion planning. It also quantifies a few issues, e.g. motor backlash, that a position controlled climbing robot may encounter.

The future work will include improving the stiffness model to incorporate pure bending moment and the compliance of motor gears. The model parameters maybe experimentally identified. Furthermore, a stiffness optimization problem can be explicitly formulated out of this model.

Acknowledgment

The authors would like to thank the efforts of Andrew Kim, Ismael, Oscar and all other team members at Robotics and Mechanisms Laboratory at UCLA.

References

[1] Salisbury, J. Kenneth. "Active stiffness control of a manipulator in Cartesian coordinates." In Decision and Control including the Symposium on Adaptive Processes, 1980 19th IEEE Conference on, pp. 95-100. IEEE, 1980.

[2] Hogan, Neville. "Impedance control: An approach to manipulation: Part II—Implementation." Journal of dynamic systems, measurement, and control 107, no. 1 (1985): 8-16.

[3] Khatib, Oussama. "A unified approach for motion and force control of robot manipulators: The operational space formulation." IEEE Journal on Robotics and Automation 3, no. 1 (1987): 43-53.

[4] Bretl, Timothy. "Motion planning of multi-limbed robots subject to equilibrium constraints: The free-climbing robot problem." The International Journal of Robotics Research 25.4 (2006): 317-342.

[5] Kumar, V., and K. J. Waldron. "Force distribution in walking vehicles." Journal of Mechanical Design 112.1 (1990): 90-99.

[6] Gao, Xiaochun, and Shin-Min Song. "A stiffness matrix method for foot force distribution of walking vehicles." Systems, Man and Cybernetics, IEEE Transactions on 22.5 (1992): 1131-1138.

[7] Gao, Xiaochun, Shin-Min Song, and Chun Qi Zheng. "A Generalized Stiffness Matrix Method for Force Distribution of Robotic Systems with

[8] Angeles, Jorge. "On the nature of the Cartesian stiffness matrix." Ingeniería mecánica, tecnología y desarrollo 3.5 (2010): 163-170.

[9] Abele, E., M. Weigold, and S. Rothenbücher. "Modeling and identification of an industrial robot for machining applications." CIRP Annals-Manufacturing Technology 56.1 (2007): 387-390.

[10] Moberg, Stig, et al. "Modeling and parameter estimation of robot manipulators using extended flexible joint models." Journal of Dynamic Systems, Measurement, and Control 136.3 (2014): 031005.

[11] Yoshikawa, Tsuneo, Atsuharu Ohta, and Katsuya Kanaoka. "State estimation and parameter identification of flexible manipulators based on visual sensor and virtual joint model." Robotics and Automation, 2001. Proceedings 2001 ICRA. IEEE International Conference on. Vol. 3. IEEE, 2001.

[12] Gosselin, Clement. "Stiffness mapping for parallel manipulators." IEEE Transactions on Robotics and Automation 6, no. 3 (1990): 377-382.

[13] Alici, Gürsel, and Bijan Shirinzadeh. "Enhanced stiffness modeling, identification and characterization for robot manipulators." IEEE transactions on robotics 21, no. 4 (2005): 554-564.

[14] Dumas, Claire, et al. "Joint stiffness identification of six-revolute industrial serial robots." Robotics and Computer-Integrated Manufacturing 27.4 (2011): 881-888.

[15] A Ghali; A.M. Neville (1972). Structural analysis: a unified classical and matrix approach. London, New York: E & FN SPON. p. 215. ISBN 0-419-21200-0.

[16] History of Strength of Materials, Stephen P. Timoshenko, 1993, Dover Publications, New York

[17] Boyd, Stephen, and Lieven Vandenberghe. Convex optimization. Cambridge university press, 2004: 95-96

Authorized licensed use limited to: UCLA Library. Downloaded on May 10,2020 at 19:46:24 UTC from IEEE Xplore. Restrictions apply.